Supplementary Information for

High-temperature ferrimagnetic order triggered metal-to-insulator transition in $CaCu_3Ni_2Os_2O_{12}$

Xubin Ye,[1,#] Yunyu Yin,[1,2,#] Yingying Cao,[1,2] Zhiyu Liao,[1] Xiao Wang,[1,2] Min Liu,[1] Qianqian Wang,[1,2] Zhao Pan,[1,2] Zhiwei Hu,[3] Hong-Ji Lin,[4] Chien-Te Chen,[4] Chih-Wen Pao,[4] Philippe Ohresser,[5] Lucie Nataf,[5] François Baudelet,[5] Wenyun Yang,[6] Jinbo Yang,[6] Jinguang Cheng,[1,2,7] Pu Yu,[8] Xianggang Qiu,[1,2,7] Yi-feng Yang,[1,2,7,*] Tao Xiang,[1,2,7] and Youwen Long[1,2,7,*]

[1]*Beijing National Laboratory for Condensed Matter Physics, Institute of Physics, Chinese Academy of Sciences, Beijing 100190, China*

[2]*University of Chinese Academy of Sciences, Beijing 100049, China*

[3]*Max Planck Institute for Chemical Physics of Solids, Dresden 01187, Germany*

[4]*National Synchrotron Radiation Research Center, Hsinchu 30076, Taiwan*

[5]*Synchrotron SOLEIL, L'Orme des Merisiers, Saint-Aubin-BP 48, 91192 Gif-sur-Yvette Cedex, France*

[6]*State Key Laboratory for Mesoscopic Physics, School of Physics, Peking University, Beijing, 100871, China*

[7]*Songshan Lake Materials Laboratory, Dongguan, Guangdong 523808, China*

[8]*State Key Laboratory of Low Dimensional Quantum Physics and Department of Physics, Tsinghua University, Beijing, 100084, China*

[#]*These authors contributed equally to this work: Xubin Ye, Yunyu Yin.*

[*]*Corresponding email: yifeng@iphy.ac.cn (Y. -F. Yang) and ywlong@iphy.ac.cn (Y. W. Long);*

Supplementary Table S1 | Structural parameters obtained from the Rietveld refinement of synchrotron XRD pattern for CCNOO at 300 K[a].

Atom	WP	*x*	*y*	*z*	*G*[b]	U_{iso} (100 × Å^2)
Ca	2*a*	0	0	0	1	0.66(7)
Cu	6*d*	0	0.5	0.5	1	0.49(2)
Ni1	4*b*	0.75	0.75	0.75	0.997(1)	0.38(1)
Os1	4*b*	0.75	0.75	0.75	0.003(1)	0.38(1)
Ni2	4*c*	0.25	0.25	0.25	0.003(1)	0.35(1)
Os2	4*c*	0.25	0.25	0.25	0.997(1)	0.35(1)
O	24*h*	0.3262(3)	0.4932(1)	0.8061(3)	1.045(5)	0.71(4)

[a]Space group *Pn*-3 (Cubic; No. 201); lattice constant a = 7.40776(1) Å. WP: Wyckoff position. G: the site occupation factor. U_{sio} represents isotropic thermal parameters. The occupancy factors of Ca, Cu, and O are fixed to be unity to refine the B/B′-site order degree for Ni/Os. Reliability factors: R_{wp} = 4.78%, R_p = 3.73%.

Supplementary Table S2 | Selected bond lengths, angles, and the BVS calculations for CCNOO obtained from the Rietveld refinement of XRD data at 300 K[a].

Parameter	Value
Cu-O (Å) (×4)	1.929(3)
(×4)	2.811(3)
(×4)	3.315(3)
Ni1−O (Å) (×6)	2.029(2)
Os2−O (Å) (×6)	1.932(2)
Cu−O−Ni1 (°)	108.2(1)
Cu−O−Os2 (°)	112.4(1)
Ni1−O−Os2 (°)	138.5(1)
BVS (Cu)	+2.09
BVS (Ni1)	+2.17
BVS (Os2)	+5.60

[a]The BVS values (V_i) were calculated using the formula $V_i = \sum_j S_{ij}$, and $S_{ij} = \exp[(r_0 - r_{ij})/b]$. In CCNOO, $r_0 = 1.649$ and $b = 0.37$ for Cu^{2+} [1], $r_0 = 1.654$ and $b = 0.37$ for Ni^{2+} [2] and $r_0 = 1.904$ and $b = 0.375$ for Os^{6+} [3]. For the A′-site Cu, 12-coordinated oxygen atoms were used, and for the B-site Ni and B′-site Os, 6-coordinated oxygen atoms were used in the BVS calculations.

Supplementary Table S3 | The spin (m_s), orbital (m_l), and total moments (m_{tot}) of the Cu 3*d*, Ni 3*d,* and Os 5*d* derived from the XMCD sum rules for CCNOO[a].

	m_s (μ_B)	m_l (μ_B)	m_{tot} (μ_B)	m_l/m_s
Cu	0.25	0.06	0.31	22%
Ni	1.12	0.31	1.43	28%
Os	-0.27	0.06	-0.21	-22%

[a]The spin and orbital moments are separately treated as follows:

$$M_{orb} = Lz = -\frac{4\int_{L_3+L_2}(\mu^+ - \mu^-)d\omega}{3\int_{L_3+L_2}(\mu^+ + \mu^-)d\omega}(10 - N_d)$$

$$M_{\text{spin}} = 2Sz + 7(Tz)$$
$$= -\frac{2\int_{L_3}(\mu^+ - \mu^-)d\omega - 4\int_{L_2}(\mu^+ - \mu^-)d\omega}{\int_{L_3+L_2}(\mu^+ + \mu^-)d\omega}(10 - N_d).$$

Here, N_d is the electron occupation number (9, 8, and 2 for Cu^{2+}, Ni^{2+}, and Os^{6+}, respectively), and $<T_Z>$ is the intra-atomic magnetic-dipole moment, which is negligible compared to M_{spin} in an octahedral (O_h) symmetry coordination[4].

Supplementary Table S4 | The calculated magnetic ground states and magnetic moments under GGA+*U*+SOC condition for CCNOO[a].

Spin structure	Calculated magnetic moment				ΔE^b (meV/f.u.)	Total theoretical moment[c] (μ_B)
	Cu/μ_B	Ni/μ_B	Os/μ_B	O/μ_B		
FM	0.68333	1.74190	1.16466	0.17885	1108.14	11
FiM1	0.54904	1.64751	-0.86509	0.02608	0	3
FiM2	-0.57541	1.71620	0.98453	0.04798	341.73	5
FiM3	-0.68741	1.60150	-1.04841	0.10290	839.16	3

[a]The table lists the magnetic moments within the muffin-tine sphere from GGA+*U*+SOC calculations with U = 5.0 eV for Cu, 4.0 eV for Ni, and 2.0 eV for Os. [b]ΔE is the energy difference between the converged magnetic configuration and the FiM1 ground state. [c]Total theoretical moment represents the ideal spin-only saturated moments for Cu^{2+} ($3d^9$, S=1/2), Ni^{2+} ($3d^8$, S=1), and Os^{6+} ($5d^2$, S=1) under initial spin structure setups.

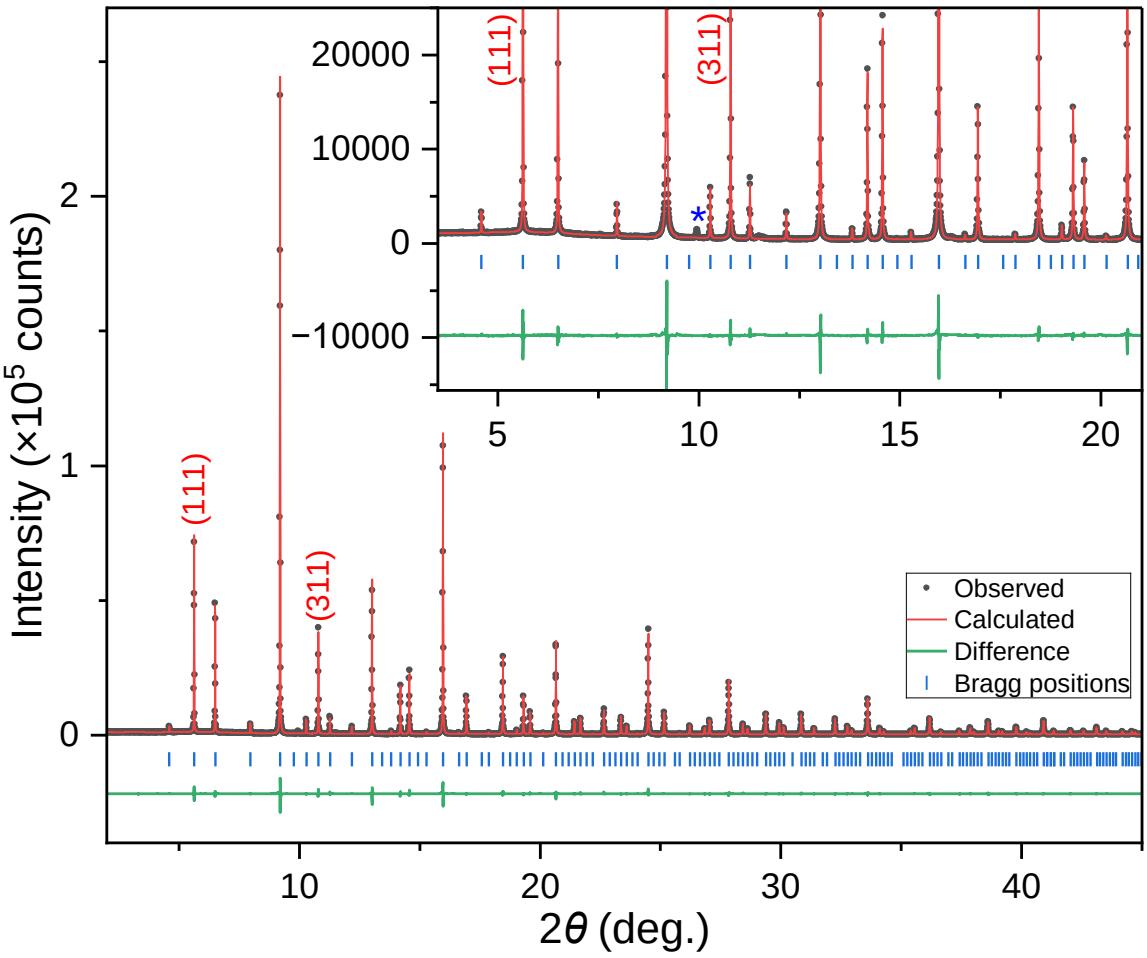

Supplementary Figure S1 | Expanded plot of SXRD pattern for CCNOO. The inset shows the data at low angles with a reduced intensity scale. A very weak impurity diffraction peak marked with asterisk, likely from OsO_2, is observed in the enlarged plot, and its intensity is about 0.3% of the strongest peak of the main phase.

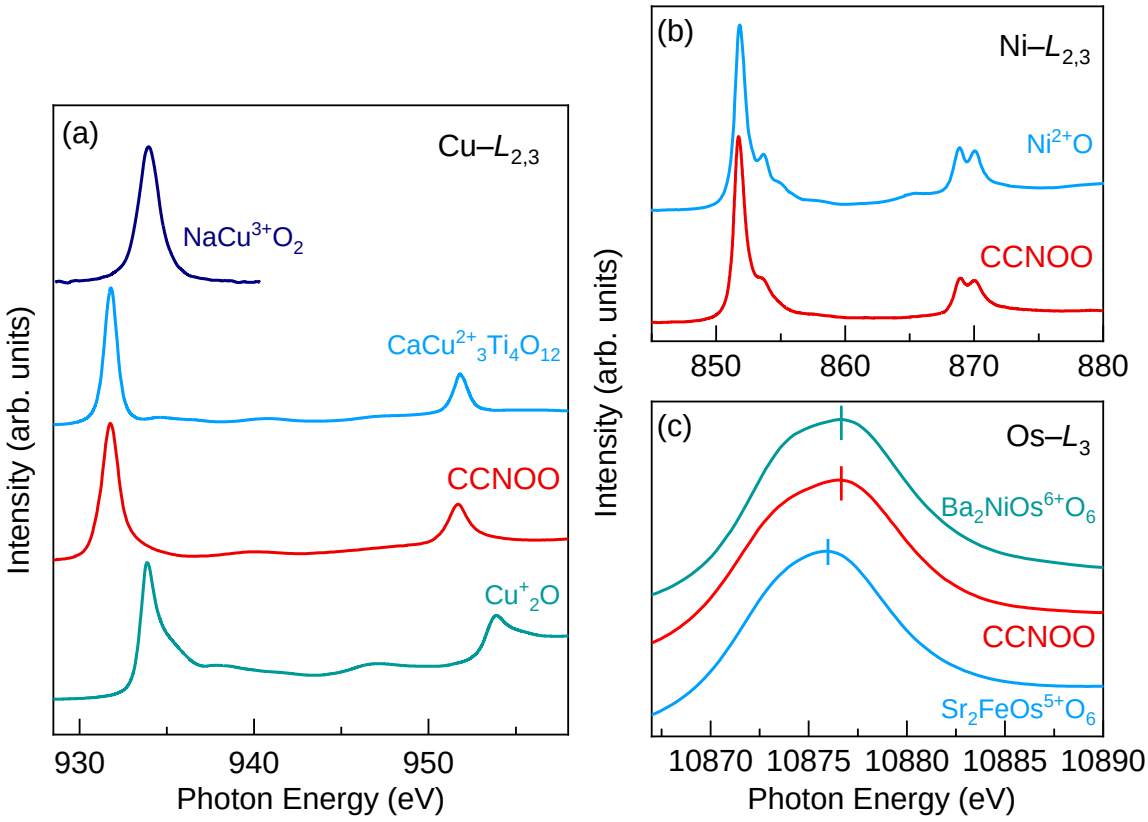

Supplementary Figure S2 | XAS spectra of CCNOO. (a) Cu-$L_{2,3}$ edges, (b) Ni-$L_{2,3}$ edges, and (c) Os-L_3 edge. The related standard reference spectra are also shown for comparison. All the Cu-, Ni-$L_{2,3}$, and Os-L_3 edges respectively exhibit very similar spectral features, such as peak energy positions and spectral shapes, to those of standard $CaCu^{2+}{}_3Ti_4O_{12}$, $Ni^{2+}O$, and $Ba_2NiOs^{6+}O_6$ references, revealing the formation of Cu^{2+}, Ni^{2+}, and Os^{6+} in CCNOO.

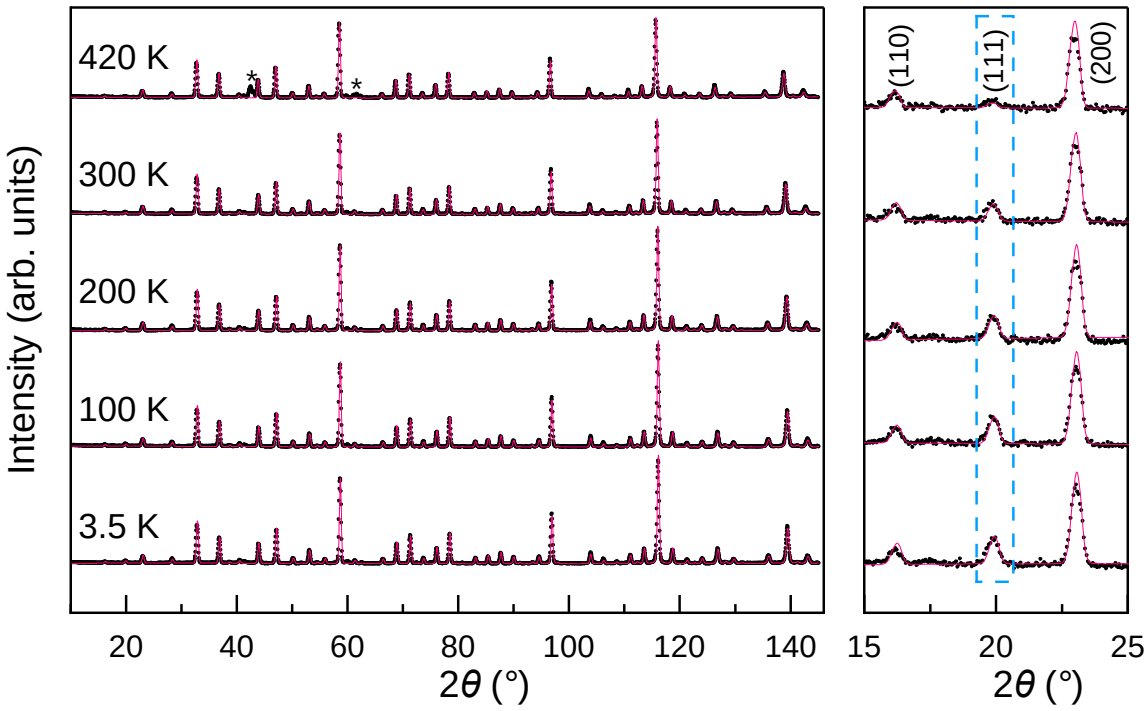

Supplementary Figure S3 | NPD patterns of CCNOO collected at selected temperatures. The right panel shows enlarged section of the pattern region containing most intense magnetic contributions, as denoted by the blue rectangular box. Because the magnetic diffraction peaks are relatively weak, only the sizable magnetic moment of Ni can directly get accurate values. To more effectively ascertain the magnetic moments of Os and Cu, we attempted to fix them at the values as measured by XMCD. We found that when the magnetic moment of Cu was fixed at 0.31 μ_B, the values for M(Os) and M(Ni) were determined as -0.20(17) μ_B and 1.81(17) μ_B, respectively. Conversely, when the magnetic moments of Os were fixed at -0.21 μ_B, the values for M(Ni) and M(Cu) were determined as 1.84(8) μ_B, and 1.04(18) μ_B, respectively. In conclusion, our refinement of the NPD data establishes the spin structure as collinear $Cu^{2+}(\uparrow)Ni^{2+}(\uparrow)Os^{6+}(\downarrow)$ FiM for CCNOO. The obtained magnetic moment values align closely with other experimental results. Note that the pattern at 420 K were measured using an aluminum container, which introduces additional diffraction peaks, as marked with asterisks.

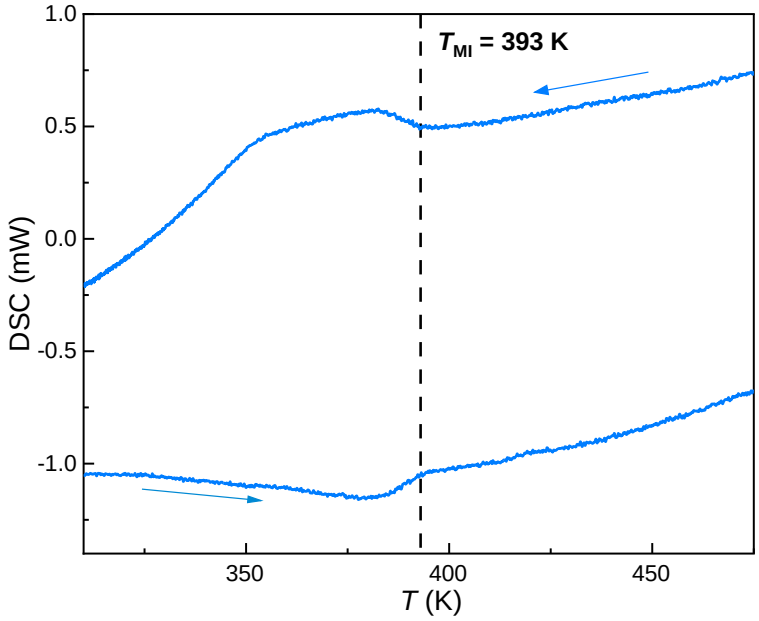

Supplementary Figure S4 | Temperature dependence of differential scanning calorimetry for CCNOO. The curves show anomaly around the critical temperature T_{MI} = T_C = 393 K without heat hysteresis during the heating and cooling processes.

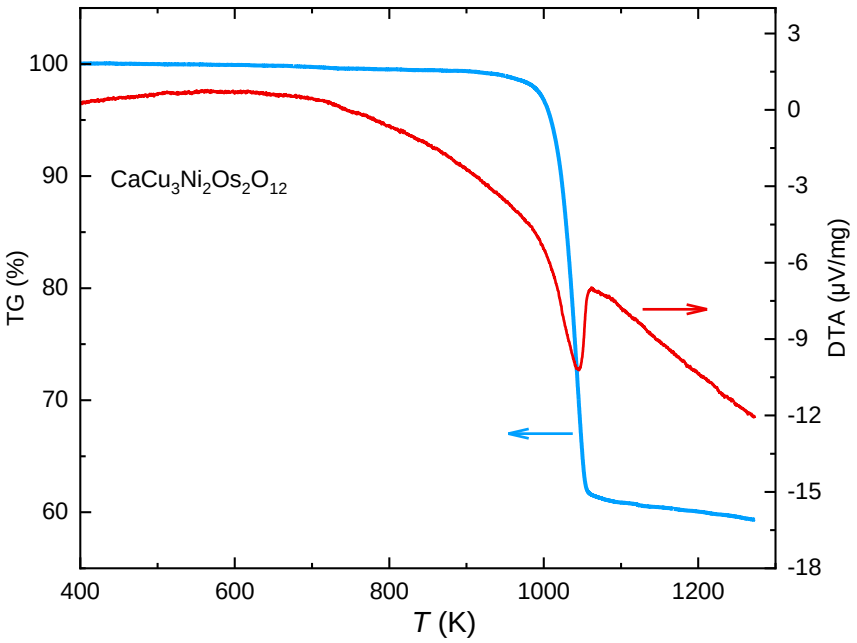

Supplementary Figure S5 | Thermogravimetry (TG) and differential thermal analysis (DTA) for CCNOO. The sample remained stable around its MIT transition and, until near 900 K, gradually decomposed into $CaOsO_3$, Cu_2O, (Cu-Ni)O, and a small amount of unknown phases. The large TG loss (~40%) is attributed to the volatilization of OsO_4 and O_2.

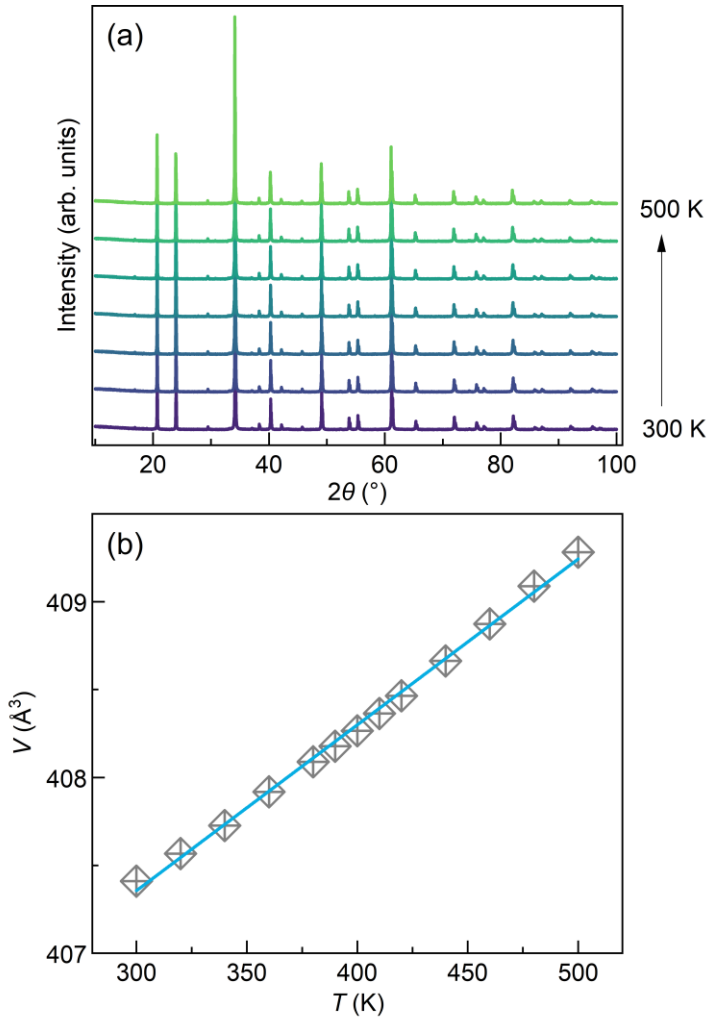

Supplementary Figure S6 | Temperature-dependent XRD patterns of CCNOO. (a) XRD patterns, and (b) Unit cell volumes in 300-500 K. The solid lines present linear fitting.

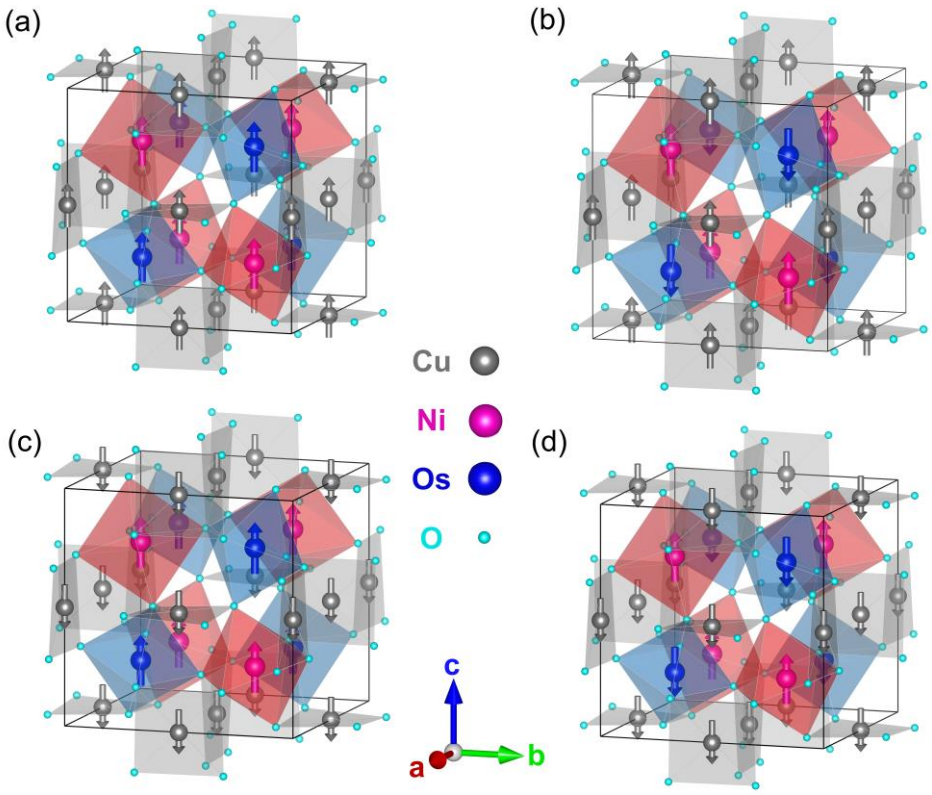

Supplementary Figure S7 | Possible spin structures of CCNOO for calculations. (a) Ferromagnetic spin structure of FM: $Cu^{2+}(\uparrow)$–$Ni^{2+}(\uparrow)$–$Os^{6+}(\uparrow)$. (b) Ferrimagnetic spin structure of FiM1: $Cu^{2+}(\uparrow)$–$Ni^{2+}(\uparrow)$–$Os^{6+}(\downarrow)$. (c) Ferrimagnetic spin structure of FiM2 $Cu^{2+}(\downarrow)$–$Ni^{2+}(\uparrow)$–$Os^{6+}(\uparrow)$. (d) Ferrimagnetic spin structure of FiM3 $Cu^{2+}(\downarrow)$–$Ni^{2+}(\uparrow)$–$Os^{6+}(\downarrow)$.

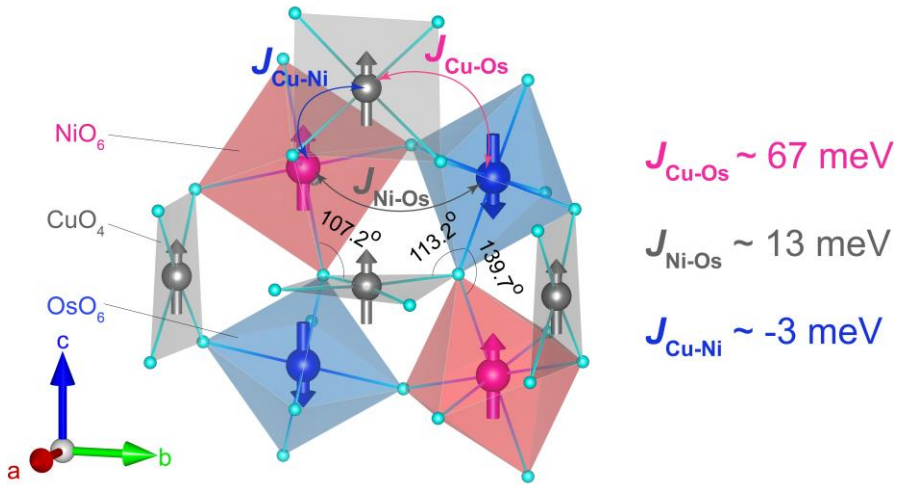

Supplementary Figure S8 | Local structure features and magnetic interactions among A′, B, and B′ sites in CCNOO. The derived exchange interactions are $J_{\text{Cu-Ni}}$ = -3 meV, $J_{\text{Ni-Os}}$ = 13 meV and $J_{\text{Cu-Os}}$ = 67 meV, supporting the FiM $Cu^{2+}(\uparrow)$-$Ni^{2+}(\uparrow)$-$Os^{6+}(\downarrow)$ spin ordering.

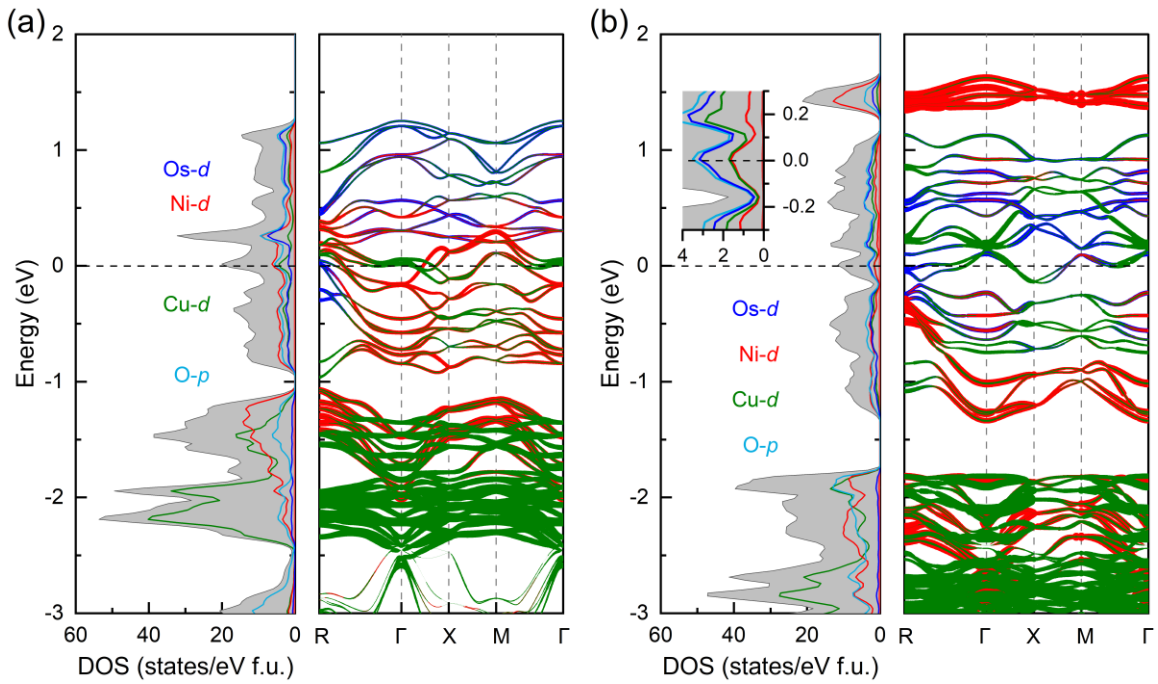

Supplementary Figure S9 | Electronic structures of non-magnetic metallic state in (a) GGA+SOC, and (b) GGA+SOC+*U* methods for CCNOO. The inset in the left panel of (b) shows the enlarged partial density of states near the Fermi level.

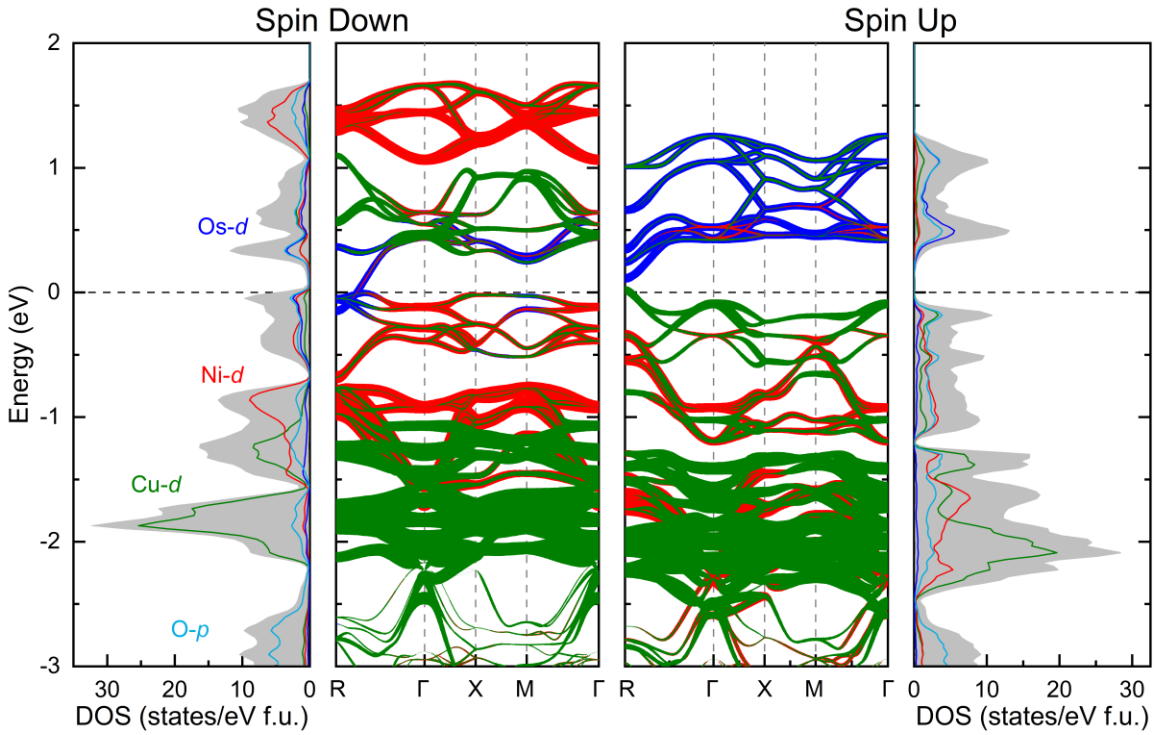

Supplementary Figure S10 | Electronic structures of GGA calculation with long-range FiM1 spin order for CCNOO. The spin order significantly renormalizes the electronic band structure, resulting in a very limited density of states near the Fermi level near the R point. The total DOS is shown by a grey line with a light grey filled area.

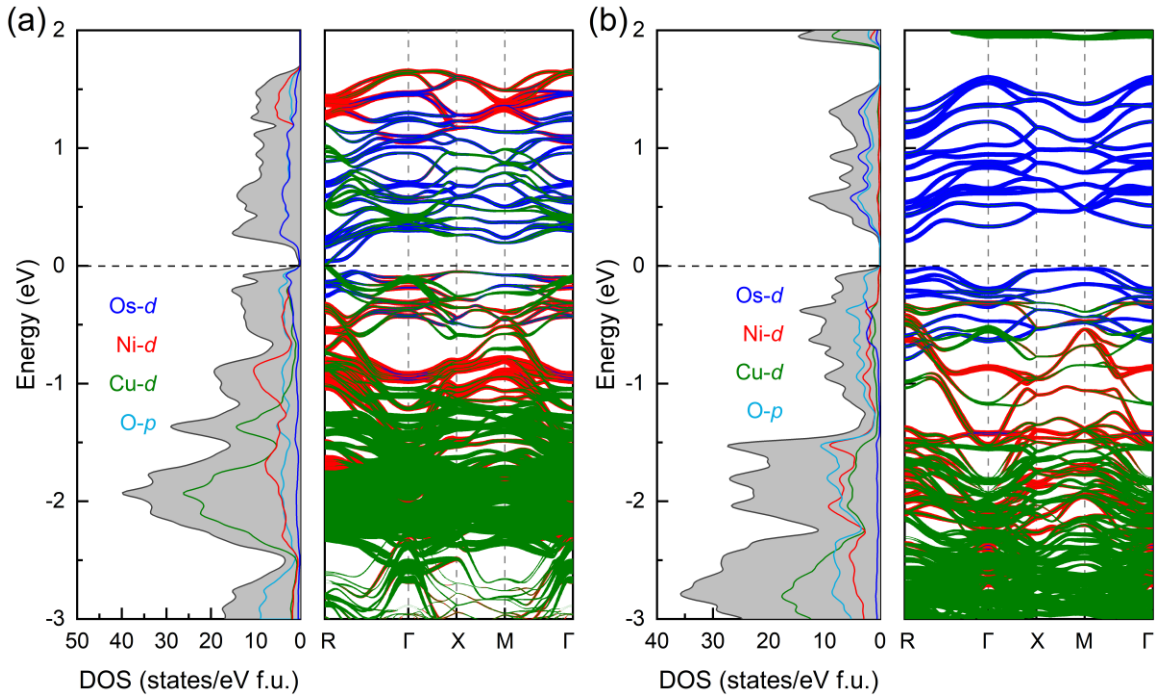

Supplementary Figure S11 | Insulating electronic structures of (a) GGA+SOC, and (b) GGA+SOC+*U* calculations with long-range FiM1 spin order. The total DOS is shown by a grey line with a light grey filled area.

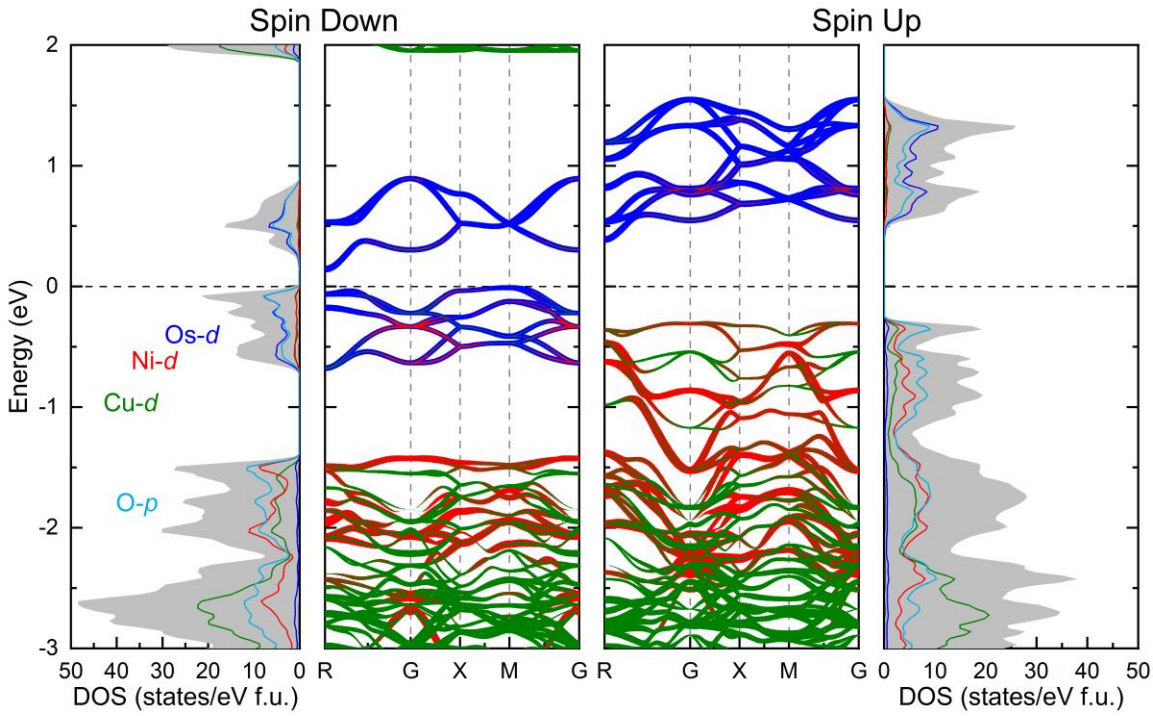

Supplementary Figure S12 | Electronic structures of GGA+*U* calculation with long-range FiM1 spin order. The total DOS is shown by a grey line with a light grey filled area.

References

1. Liu, W. & Thorp, H. H. Bond valence sum analysis of metal-ligand bond lengths in metalloenzymes and model complexes. 2. Refined distances and other enzymes. *Inorg. Chem.* **32**, 4102–4105 (1993).
2. Brown, I. D. & Altermatt, D. Bond-valence parameters obtained from a systematic analysis of the Inorganic Crystal Structure Database. *Acta Crystallogr. B* **41**, 244–247 (1985).
3. Gagné, O. C. & Hawthorne, F. C. Comprehensive derivation of bond-valence parameters for ion pairs involving oxygen. *Acta Crystallogr., Sect. B: Struct. Sci., Cryst. Eng. Mater.* **71**, 562–578 (2015).
4. Carra, P., Thole, B. T., Altarelli, M. & Wang, X. X-ray circular dichroism and local magnetic fields. *Phys. Rev. Lett.* **70**, 694–697 (1993).